

# Regulation Signal Design and Fast Frequency Control with Energy Storage Systems

Noela Sofia Guzman E., *Student Member, IEEE*, Mariano Arriaga, *Member, IEEE*,  
 Claudio A. Cañizares, *Fellow, IEEE*, John W. Simpson-Porco, *Member, IEEE*, Daniel Sohm, *Member, IEEE*,  
 and Kankar Bhattacharya, *Fellow, IEEE*

**Abstract**—This paper presents a novel  $\mathcal{H}_2$  filter design procedure to optimally split the Frequency Regulation (FR) signal between conventional and fast regulating Energy Storage System (ESS) assets, considering typical Communication Delays (CDs). The filter is then integrated into a previously validated FR model of the Ontario Power System (OPS) including Battery and Flywheel ESSs, which is used to analyze the impact of these ESSs, CDs, and limited regulation capacity in the FR process in a real system. The proposed methodology to split the FR signal is also compared with the existing FR process, with the results showing that the proposed  $\mathcal{H}_2$  filter design and signal splitting strategy can improve the FR process performance significantly, in terms of reducing the Area Control Error (ACE) signal, and thus reduce the need for regulation capacity.

**Index Terms**—Batteries, energy storage, flywheels, frequency regulation, frequency control, regulation signal.

## NOMENCLATURE

### Indices

$ESS$	ESS: FESS or BESS.
$i$	Elements in $W(z)$ .
$j$	Elements in $Z(z)$ .

### Parameters

$AV_{ESS}$	Status availability of the ESS.
$CD$	Communication delay ( $z^{-\tau}$ ), where $\tau$ is an integer representing the delay in seconds.
$P_D$	Load of the system [MW].
$P_{GT}$	Generation total dispatch [MW].
$RC_{ESS}$	ESSs FR capacity limit [MW].
$RC_{TG}$	TGs FR capacity limit [MW].
$RC$	FR capacity limit [MW].
$B$	BA bias [MW/0.1Hz].
$f_s$	Scheduled frequency [Hz].

This work was supported by the NSERC Energy Storage Technology (NEST) Network. The energy storage data was kindly provided by NRStor Inc. under the auspices of an experimental research program facilitated by Ontario's Independent Electricity System Operator (IESO).

N. S. Guzman, C. A. Cañizares, and K. Bhattacharya are with the Department of Electrical and Computer Engineering, University of Waterloo, Waterloo, ON, N2L 3G1, Canada (e-mail: nguzman@uwaterloo.ca; ccanizares@uwaterloo.ca; kankar.bhattacharya@uwaterloo.ca).

M. Arriaga is with the Energy and Power Innovation Centre at Mohawk College, Hamilton, ON, L9C 0E5, Canada (e-mail: mariano.arriaga@mohawkcollege.ca).

J. W. Simpson-Porco is with the Department of Electrical and Computer Engineering, University of Toronto, Toronto, ON, M5S 3G4, Canada (e-mail: jwsimpson@ece.utoronto.ca).

D. Sohm is with the Independent Electricity System Operator (IESO) of Ontario, Toronto, ON, M5H 1T1, Canada (e-mail: Daniel.Sohm@ieso.ca).

$I$	Identity matrix.
$IME$	Interchange metering error [MW].
$IP$	Inadvertent payback [MW].
$NI_s$	Scheduled net interchanges [MW].
Variables	
$\alpha_{ESS}$	Factor indicating the capacity contribution of the ESS to $RC_{ESS}$ [p.u.]
$\overline{M}_{ESS}$	Maximum available capacity of the ESS [MW].
$\underline{M}_{ESS}$	Minimum available capacity of the ESS [MW].
$ACE_{filtered}$	ACE filtered signal [MW].
$BP_{ESS}$	ESS fixed base point [MW].
$BPm_{ESS}$	ESS moving base-point [MW].
$F(IP)$	Function of inadvertent payback [MW].
$P_{TGr}$	Output power of TG contracted for FR [MW].
$SOC_{ESS}$	ESS SoC [%].
$SP_{ESS}$	ESS SP signal [MW].
$SR$	Scheduled FR signal [MW].
$SR_{ESS}$	ESS regulation signal [MW].
$\Phi$	Controller/Filter.
$\Phi_W, \Phi_Z$	Weighting filters associated to the input $W$ and output $Z$ , respectively.
$A, B, C, D$	State-space matrix representation of the transfer function matrix $GP(z)$ .
$ACE$	Area Control Error [MW].
$Clp$	Clamping signal.
$f_a$	Actual frequency [Hz].
$GP(z)$	Generalized Plant transfer function matrix
$N(z)$	Lower linear fractional transformation of $\Phi(z)$ around $GP(z)$ .
$NI_a$	Actual net interchanges [MW].
$P_{ESS}$	Power output of the ESS [MW].
$RegA$	Traditional Regulation Signal [MW].
$RegA_L$	Traditional Regulation Signal limited [MW].
$RegD$	Dynamic Regulation Signal [MW].
$RegD_L$	Dynamic Regulation Signal limited [MW].
$U$	Control signals.
$U_1$	$RegA$ as control signal.
$U_2$	$RegD$ as control signal.
$W$	(Weighted) exogenous inputs/disturbance input vector.
$Y$	Sensed outputs.
$Y_1$	ACE as sensed output.
$Y_2$	Cumulative ACE as sensed output.
$Z$	(Weighted) exogenous outputs/error output vector.

## I. INTRODUCTION

**T**HE inherent variability and increasing penetration of Renewable Energy Sources (RESs) in power systems have the potential to negatively impact the system frequency. Fast power response Energy Storage System (ESS) technologies can mitigate frequency variations when included in the Frequency Regulation (FR) control loop [1]. Furthermore, ESS technology applications to power grids such as FR are becoming feasible with their increasing technical maturity and lower cost trends; however, they still have to overcome issues such as limited power and energy capacities, given the continuous nature of the FR process, for a desired standard of FR performance.

Joint efforts from electricity regulators, technology developers, and Independent System Operators (ISOs) have led to the development of new services and control approaches to exploit the unique characteristics and potential benefits of fast responding technologies such as Battery Energy Storage Systems (BESSs) and Flywheel Energy Storage Systems (FESSs) [2]–[5]. Regulatory changes have been introduced to ease the participation of ESS in energy, capacity, and ancillary service markets [6], and promote a performance-based payment approach for FR to incentivize the integration of fast response ESS technologies [2]. An example of the latter is the Federal Energy Regulatory Commission (FERC) Order No.755, which led to changes in the U.S. market design and requires a two-part compensation for FR reserves: capacity and performance payment [7]. The performance payment, which has been incorporated in various ways in different ISOs, is also known as mileage payment and is a compensation for the movement (speed and accuracy) of the facility in response to Automatic Generation Control (AGC) signals [8], [9].

In addition, some ISOs are considering measures to support the integration of ESS within their administered markets [10], or have procured or already implemented FR-ESS-related projects [5], [7]. For instance, the California Independent System Operator (CAISO) includes ESS within a set of resources called non-generating resources, which can be non-Regulation Energy Management (REM) resources and be subject to the same conditions as traditional generators to meet a 60 minute continuous energy requirement, or be REM resources with an energy requirement of 15 minutes [11]. In the New York Independent System Operator (NYISO), the ESSs are called Limited Energy Storage Resources (LESR), and are assigned their regulation base point based on their State of Charge (SoC) every 5 minutes [8].

To use the fast response capability of some ESS beyond the traditional AGC framework, some ISOs have introduced a much faster regulation signal, compared to the traditional one, with the resources following this signal receiving extra payment [11]. For instance, PJM considers the participation of ESS in its FR market and offers two regulation AGC signals: a Traditional Regulation Signal (*RegA*) meant for traditional generators with limited ramp rate, and a Dynamic Regulation Signal (*RegD*) meant for high ramp rate capability units. The signal *RegD* is derived from the same algorithm as *RegA*, but *RegD* filters out low-frequency components, resulting in a

fast cycling signal [7], [8]. The Independent System Operator of New England (ISONE), which includes ESS facilities in their Alternative Technology Regulation Resources, has two faster energy neutral signals (energy-neutral continuous and energy neutral trinary) meant for alternative technologies, and also sends a slower AGC signal to conventional facilities every four seconds [11], [12]; these signals behave similarly to PJM's *RegD* and *RegA* [11]. The Midcontinent Independent System Operator (MISO) also has an AGC-enhanced signal for fast ramping resources specifically to allow ESSs, referred to as short term Storage Energy Resources, to participate in the regulation reserve market and to improve the use of fast ramping facilities [9].

In recent years, ISOs have implemented strategies to split the FR signal between conventional and fast assets considering economic and operational factors such as market aspects, system stability, and performance [3], [7]. These initial attempts have resulted in FR improvements that reduced FR procurement requirements [11]; however, only a limited amount of technical information is publicly available for the ISOs' implemented strategies, with only block diagrams and no detailed information about their design or tuning processes [13]. Thus, it is impractical to target the optimization of such split signal strategies without the detailed design data. Furthermore in [14], detailed information regarding different filtering topologies and design considerations for Chebyshev-based filters are presented, but the model only considers an open-loop process which does not account for the closed-loop feedback effects of the filter outputs in the FR control loop. In this paper, the split signal optimization and closed-loop components are considered in the proposed FR signal model.

The participation of Traditional Generators (TGs) and ESSs in primary FR and the role of ESS in recovering the SoC in the secondary FR process is examined in [15]. A BESS control strategy to improve the dynamic performance of AGC is studied in [16]. In [17], the split of Area Control Error (ACE) among TGs and BESS using an index that captures the available FR capability of a BESS is proposed, while the scheduling of TGs and ESS based on Control Performance Standard 1 (CPS1) compliance is reported in [18]. However, Communication Delays (CDs) or mathematical models of the SoC of the ESS, which are not all jointly included in any of the aforementioned works, have the potential to impact the FR performance [19], [20].

From the aforementioned literature review, it can be concluded that the actual benefits of ESSs can be only realized if there is an appropriate filtering strategy for the FR signal, splitting the FR signal into a slow and a fast component, while considering operational limitations, which is still a work in progress. Therefore, the present paper contributes to the on-going efforts of FR design and system impact studies considering fast acting ESSs as follows:

- A novel  $\mathcal{H}_2$ -filter design procedure is proposed to optimally split the FR signal into fast and slow components, to improve the FR performance in terms of minimizing ACE variations. This presents an advantage with respect to existing approaches, where currently no optimization

or systematic tuning procedures, if any, are publicly available.

- The proposed FR signal filter is integrated into a previously validated Ontario Power System (OPS) FR simulation model that includes CDs and ESSs, including SoCs, to form an Integrated Model of the FR process. The Integrated Model accounts for the closed-loop feedback effects of the outputs of the filter in the frequency control process, which are not considered in existing practical models based on open-loop system representations.
- The application of the proposed Integrated Model to the OPS is used to demonstrate the expected impact of fast response ESSs on the FR process, accounting for and evaluating the effect of CDs and limited regulation capacity, which have not been both considered in practical systems before.

The rest of the paper is organized as follows: Section II briefly discusses fast FR in power systems, presents an overview of ESS technologies used for such services, and briefly describes the previously developed and validated FR simulation model that is used as the Base Case. Section III details the FR signal filter design and its integration in the Base Case Model to develop the proposed Integrated Model. Section IV presents simulation results and discussions of a validated model of the Ontario grid, demonstrating the impact of CDs and limited capacity on the FR process. Finally, Section V highlights the main conclusions and contributions of the paper.

## II. BACKGROUND

### A. FR in Power Systems

FR in power systems refer to the dynamic control loop that maintains the system frequency at 50/60 Hz, given a predefined tolerance, by maintaining the power generation and load balance in the system [21]. As part of the FR process, the control loop calculates the ACE, which is the instantaneous mismatch between the measured and scheduled interchange, considering the frequency bias effect and, the meter error correction, and is given by [22]:

$$ACE = (NI_a - NI_s) - 10B(f_a - f_s) - IME \quad (1)$$

where all the parameters and variables in this and other equations and models are defined in the nomenclature section. This generalized equation is used in an interconnected system where each Balancing Authority (BA) is assigned FR responsibilities. The resulting FR signal, based on the ACE, is sent to the assigned regulating assets at specified time intervals, which depending on the system complexity, technology used, and/or size, can be 2 to 4 s for large grids [22].

ESS grid-scale projects have been deployed to support FR services in different systems [3]. The maturity of BESS and FESS technology has opened the door to analyze and implement strategies taking advantage of their fast response characteristic, and various studies have analyzed the technical benefits and capacity limits of different fast regulating assets while complying with the performance standards (e.g., [4]).

In general, ISOs' FR strategy has evolved to allow for more than one regulation signal depending on the assets' ramp rate constraints. For example, a traditional or slow changing FR signal is sent to conventional generators (e.g., hydro power and gas turbines); while fast changing assets, such as FESS and BESS, are sent a faster changing FR signal that accounts for the higher ramp rates of these technologies [3].

### B. Fast FR Technologies

FESS and BESS have been widely deployed for FR services due to their fast response characteristic [23]–[25]. FESSs are well suited for FR applications since they have a very high cycle life (hundred of thousands of cycles), a long operational life (about 20 years), high round trip efficiency (up to 95%), high power density, insensitivity to deep discharges, fast response time (ms), discharge times of seconds to minutes, and are environmentally safe and have modular characteristics [24], [25]. Also, cost reduction trends, power/energy modularity, and industry competition have made batteries and BESS a feasible technology for on-grid ancillary services and off-grid applications [24]. Depending on the type of battery (conventional, advanced, metal air, or flow), the round trip efficiency varies between 60% and 95%, discharge times are from seconds to hours, response times are in the order of ms, and have lifetimes of up to 25 years [24], [25]. However, despite all the characteristics that make these ESS technologies suitable for FR provision, both FESSs and BESSs have a limited storage capacity that impact the provision of FR services, as analyzed in this paper.

### C. FR Model

The dynamic model used here for FR studies is explained in detail in [26], and corresponds to a large interconnected power system with ESS, which in 2020 had a peak demand of 24.4 GW [27], and a typical FR scheduled capacity of  $\pm 100$  MW [28]. This dynamic model, which is illustrated in Fig. 1 and referred to as the Base Case Model in this paper, considers all relevant stages in the FR control process. The bulk power system and ESSs, particularly FESS and BESS, are modeled in detail from a FR perspective, including the ESS SoC management model. Furthermore, CDs in the signals sent from/to the control center to/from the facilities contracted for FR are also considered. This model has been validated using a practical transient stability model of the North American Eastern Interconnection (NAEI), and real data of the OPS, including a 2 MW/0.5 MWh FESS, and a 4 MW/2.76 MWh BESS, used for FR provision by the Independent Electricity System Operator (IESO) of Ontario. For the proposed Integrated Model, the BESS and FESS capacity has been scaled up to properly analyze the impact of fast regulation in the Ontario system. The real data used for the validation of the Base Case Model has resolution of 1 s.

The Base Case Model in Fig. 1 has two group blocks: Bulk System and ESS. The first block in the Bulk System group block is the ACE calculation, whose input signals are  $NI_a$ ,  $f_a$ ,  $NI_s$ ,  $f_s$ ,  $IP$ , and  $IME$ . A function of  $IP$ ,  $F(IP)$  is included

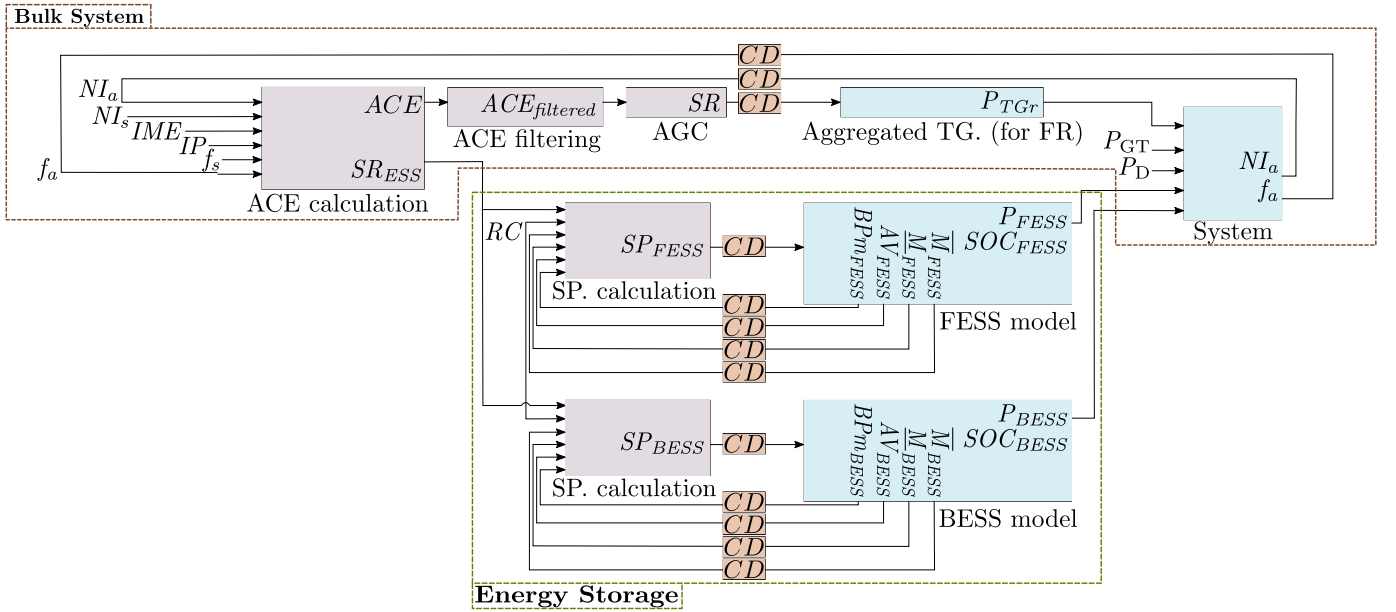


Fig. 1: Validated FR simulation model of a bulk power system with ESS (Base Case Model) [26].

in this block to represent the differences between the ACE measured data and model results, and the output signals of this block are the  $ACE$  and  $SR_{ESS}$  signals. The  $ACE$  signal enters an existing ACE filtering block, which removes fast signal changes that TGs are not able to react to, and outputs the  $ACE_{filtered}$  signal. This signal enters the AGC block, whose purpose is to calculate the  $SR$  signal sent to the aggregated model of the TGs contracted for regulation. The output of this block,  $P_{TGr}$ , together with  $P_D$ ,  $P_{GT}$ ,  $P_{FESS}$  and  $P_{BESS}$  are sent to the system block. The latter, which represents the primary frequency response of the elements in the system and the tie-lines power, uses these inputs to calculate the signals  $NI_a$  and  $f_a$ , and then sends them back to the ACE calculation block, closing the FR control loop.

The ESS group block includes two blocks. The first block is the Set-Point (SP) calculation block, which receives the  $SR_{ESS}$  signal from the ACE calculation block,  $RC$ , and  $AV_{ESS}$ ,  $BPm_{ESS}$ ,  $\overline{M}_{ESS}$ , and  $\underline{M}_{ESS}$  signals from the ESS models. The SP calculation block outputs the SP signal  $SP_{ESS}$ , which is later sent to the ESS facilities, i.e., FESS and BESS, and is in essence a scaled version of the  $SR_{ESS}$  signal taking into account the SoC of the ESS facilities. The second block in the ESS section corresponds to the ESS model of the facility, including their SoC management model, yielding  $P_{ESS}$ ,  $SOC_{ESS}$ ,  $\overline{M}_{ESS}$ ,  $\underline{M}_{ESS}$ ,  $AV_{ESS}$ , and  $BPm_{ESS}$ . These last four signals are fed back to the SP calculation block considering CDs.

Observe that the FR signals sent from the control center to TGs and ESS facilities are created independently from each other, thus there is the need for a coordinated control of these signals, as proposed in this paper.

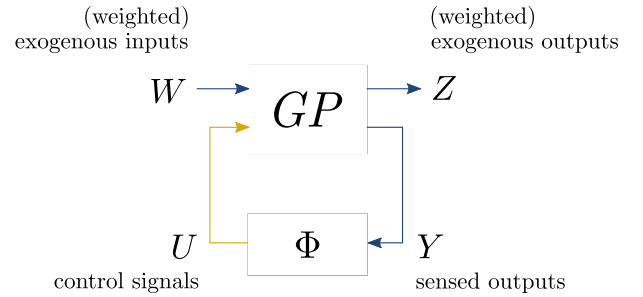


Fig. 2: General control problem formulation.

### III. DESIGN OF $\mathcal{H}_2$ FILTER FOR FR SIGNAL

#### A. Filter Design

The design approach used here is to filter the FR signal by producing a slowly-varying component or  $RegA$  to be provided to the slow regulating resources, while the remaining fast component or  $RegD$  is provided to the fast regulating facilities, as in the PJM electricity market [7]. This is done to take advantage of the fast changing power output characteristic of ESSs in the FR control loop. Hence, it is assumed here, as per general practices, that fast response ESS technologies, i.e., FESS and BESS, receive the  $RegD$  signal due to their fast response characteristics. Slower types of ESS technologies such as compressed-air and thermal ESSs can also be added to the FR control loop, receiving the  $RegA$  signal due their prolonged discharging and slower power output characteristics.

The design of the filter is formulated as an optimal control design problem, based on the general control configuration shown in Fig. 2, consisting of a Generalized Plant (GP) transfer function  $GP(z)$ , which includes weights, interconnected with a controller  $\Phi(z)$ . The controller  $\Phi(z)$  processes the available measurements  $Y$  to produce the control signal  $U$ . The signal  $W$  models exogenous inputs/disturbances, and the

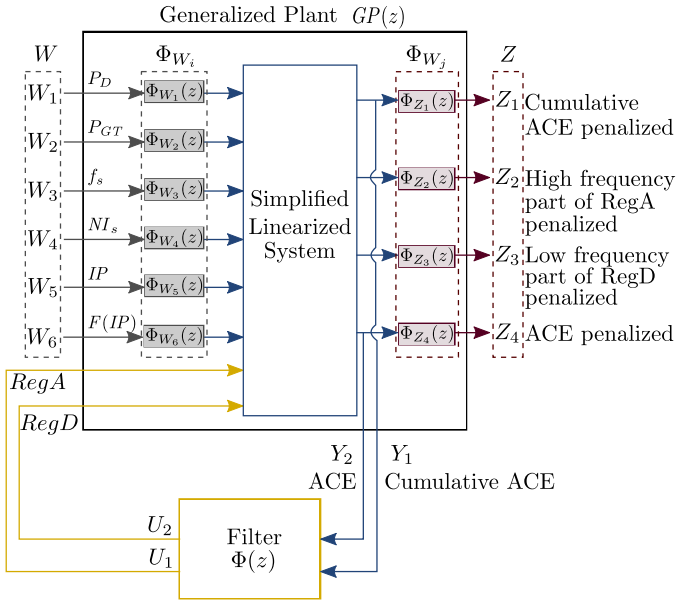


Fig. 3: Optimal control configuration.

signal  $Z$  contains controlled variables that the designer wishes to keep small [29]. The blocks can be represented by the transfer matrix relationship

$$\begin{bmatrix} Z \\ Y \end{bmatrix} = \begin{bmatrix} GP_{11}(z) & GP_{12}(z) \\ GP_{21}(z) & GP_{22}(z) \end{bmatrix} \begin{bmatrix} W \\ U \end{bmatrix} \quad (2)$$

$$U = \Phi(z)Y \quad (3)$$

The control problem is to design  $\Phi(z)$  such that the  $\mathcal{H}_2$  norm of the closed-loop transfer function from  $W$  to  $Z$ , given by  $GP_{11}(z) + GP_{12}(z)\Phi(z)(I - GP_{22}(z)\Phi(z))^{-1}GP_{21}(z)$ , is minimized in the  $\mathcal{H}_2$  sense; see, e.g., [29] for a formal definition of the  $\mathcal{H}_2$  norm. Effectively, this procedure minimizes the sensitivity transfer function from  $W$  to  $Z$ , thereby suppressing the effect of the exogenous disturbances  $W$  on the controlled variables  $Z$ . Under standard technical assumptions, this control problem is solvable via routine computational methods [29] which are implemented in Matlab [30].

The design of the proposed filter for FR is now cast into this general framework, as shown in Fig. 3. The signals  $Y_1$  and  $Y_2$  correspond to ACE and cumulative ACE signals, which are the plant measurement outputs provided to the controller;  $U_1$  and  $U_2$  correspond to  $RegA$  and  $RegD$ , which are the control inputs the filter produces (the outputs of the filter). The generalized plant  $GP(z)$  illustrated in Fig. 4 is constructed from the simplified nonlinear version of the Base Case FR Model depicted in Fig. 1 through the following steps. First, all signal loops that would enter the new filter  $\Phi(z)$  are broken by removing the ACE filtering and AGC blocks. Next, nonlinearities such as limiters are removed, and all ESS systems are approximated as ideal set-point followers; this is done to obtain a simplified linear time-invariant model. Finally, the exogenous inputs  $W$  and performance outputs  $Z$  are identified, and associated weighting filters  $\Phi_{W_i}(z)$  and  $\Phi_{Z_j}(z)$  are added, where  $i$  and  $j$  are associated with each element in  $W$  and  $Z$ , respectively. The exogenous disturbance

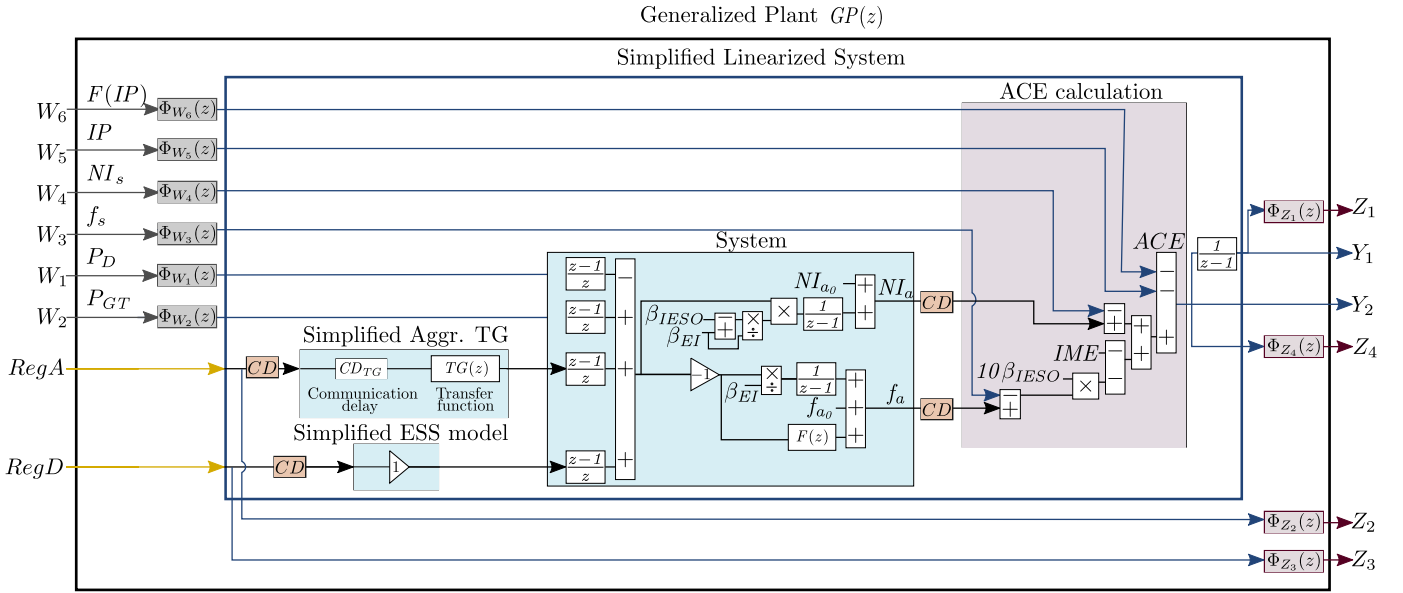
vector  $W$  models the inputs  $[P_D \ P_{GT} \ f_s \ NI_s \ IP \ F(IP)]^T$ . The vector signal  $Z = [Z_1 \ Z_2 \ Z_3 \ Z_4]^T$  contains the error outputs to be kept small, which corresponds to cumulative ACE, high frequency component of  $RegA$ , low frequency component of  $RegD$ , and ACE signals, which are penalized by the  $\Phi_{Z_1}(z)$  to  $\Phi_{Z_4}(z)$  filters. The state-space representation of  $GP(z)$  is obtained by implementing the model in Fig. 4 in Simulink<sup>®</sup> and by using the Matlab function `linearize`, which yields the matrices  $A$ ,  $B$ ,  $C$ , and  $D$  corresponding to the state space representation at time zero of the transfer function  $GP(z)$  in (2). The dimensions of the state-space matrices for the case with delays are  $A_{50 \times 50}$ ,  $B_{50 \times 8}$ ,  $C_{6 \times 50}$ , and  $D_{6 \times 8}$ , while for the case without delays are  $A_{12 \times 12}$ ,  $B_{12 \times 8}$ ,  $C_{6 \times 12}$ , and  $D_{6 \times 8}$ .

The various filters  $\Phi_{W_i}(z)$  and  $\Phi_{Z_j}(z)$  in Fig. 3 are not physically present, but are design variables of the optimal control problem. These filters specify the magnitude of the disturbance/error signals, and allow to shape the closed-loop response by weighting the importance of disturbances and error variables over desired frequency ranges.

The filters  $\Phi_{W_i}(z)$  are selected as constant gains here, based on the largest change observed in the real data provided by the IESO for each input  $i$ . The filters  $\Phi_{Z_1}(z)$  and  $\Phi_{Z_4}(z)$  are selected as constant gains. The  $RegD$  signal should contain relatively little low-frequency content, while the  $RegA$  signal should contain relatively little high-frequency content, and hence,  $\Phi_{Z_2}(z)$  and  $\Phi_{Z_3}(z)$  include a constant gain multiplying a high-pass and low-pass filter, respectively. The high-pass filter penalizes the high frequency content in  $RegA$ , while leaving the low frequency behaviour unchanged. Conversely, the low-pass filter discourages high frequency content in  $RegD$ , which encourage ESS facilities to provide a fast power response. The high- and low-pass filters can be determined based on the analysis of the discrete Fourier transform of the measured ACE signal. Furthermore, all the constant gains present in the filters  $\Phi_{Z_j}(z)$  can be determined using a recurrent process, which included a Genetic Algorithm (GA) described next.

The first GA step is to set the initial individual, which corresponds to the set of constant gains in  $\Phi_{Z_j}(z)$ ; these gains together with the  $\Phi_{W_i}(z)$  filters selected are then inserted in  $GP(z)$ . The filter  $\Phi(z)$  is generated using the Matlab function `h2syn` that computes a stabilizing  $\mathcal{H}_2$ -optimal controller  $\Phi(z)$  for the plant  $GP(z)$  [30]. Next,  $\Phi(z)$  is added to the Base Case Model to arrive at an Integrated Model, described below, and the Root Mean Squared Error (RMSE) of the ACE signal for a one day period is calculated. The GA determines the next individual, and the process continues until the stopping criteria is met and the individual that yields the lowest RMSE of ACE is selected.

The solution to the optimal control problem illustrated in Fig. 3 requires that one appropriately selects the weighting filters  $\Phi_{W_i}$  and  $\Phi_{Z_j}$ . The computation of the filter  $\Phi(z)$  that minimizes the norm of the transfer function from  $W$  to  $Z$  (while guaranteeing stability of the linear system) can then be systematically solved via standard methods in either  $\mathcal{H}_2$  or  $\mathcal{H}_\infty$  frameworks, as explained in [29]. In this study, the  $\mathcal{H}_2$  synthesis procedure produced better results compared to

Fig. 4: Simplified Linearized System and Generalized Plant  $GP(z)$ 

the  $\mathcal{H}_\infty$  procedure, as measured by smaller RMSE and Mean Absolute Error (MAE) of the ACE signal for the simulation studies presented in Section IV, and hence only the results for the  $\mathcal{H}_2$  filter design are described in what follows.

### B. Filter Integration

The Integrated Model shown in Fig. 5 corresponds to the Base Case FR Model in Fig. 1 with some modifications and the addition of the proposed  $\mathcal{H}_2$  filter. The modifications, presented in green, include a Proposed Set-Point (PSP) calculation replacing the SP calculation block, and the substitution of the ACE filtered and AGC blocks by the designed filter. The  $\mathcal{H}_2$  filter is implemented using its state-space representation, which has two input signals: ACE and cumulative ACE, and two outputs:  $RegA$  and  $RegD$ , which go through a limiter block. Thus,  $RegA_L$  corresponds to  $RegA$  limited between  $\pm RC_{TG}$ , which is the FR capacity of TGs, and  $RegD_L$  is  $RegD$  limited between  $\pm RC_{ESS}$ , which is the FR capacity of fast response resources. The  $RC_{ESS}$  is obtained by adding the FESS and BESS FR capacity limits  $RC_{FESS}$  and  $RC_{BESS}$ , respectively.

Since the Integrated Model considers limited FR capacity and the SoC model of the facilities, six cases are possible, depending on whether the TGs are limited or not, and depending on whether the ESS is limited, SoC limited, or neither. Within these six cases, two extreme cases can arise: both TGs and ESSs reach their limits, or TGs reach their limit while the ESS facilities are not able to follow the SP signals because of their SoC limits. If these two extreme cases arise and the load-generation mismatch increases, the filter will receive increasing ACE and cumulative ACE signals, hence increasing the requirement from the regulation resources through  $RegA$  and  $RegD$ . However, since the facilities are not able to follow their SP signals, the error will keep accumulating, and the requirement from the facilities will continue increasing.

This saturation in the filter is an issue that can be corrected by implementing the following conditional integration anti-windup strategy:

$$Clp =$$

$$\left\{ \begin{array}{l} 1 \quad \forall \{ [(RegD_L < 0 \wedge \underline{M}_{FESS} = BP_{FESS}) \vee \\ (RegD_L \geq 0 \wedge \overline{M}_{FESS} = BP_{FESS})] \wedge \\ [(RegD_L < 0 \wedge \underline{M}_{BESS} = BP_{BESS}) \vee \\ (RegD_L \geq 0 \wedge \overline{M}_{BESS} = BP_{BESS})] \wedge \\ (RegA > RC_{TG} \vee RegA < -RC_{TG}) \wedge \\ [sgn(-RegA) = sgn(ACE)] \wedge \\ [sgn(-RegD) = sgn(ACE)] \} \vee \\ \{ (RegA > RC_{TG} \vee RegA < -RC_{TG}) \wedge \\ (RegD > RC_{ESS} \vee RegD < -RC_{ESS}) \wedge \\ [sgn(-RegA) = sgn(ACE)] \wedge \\ [sgn(-RegD) = sgn(ACE)] \} \\ 0 \quad \text{otherwise} \end{array} \right. \quad (4)$$

where  $Clp$  can be equal to 1 or 0, depending on the stated logic conditions, which consider the values and signs of  $RegD_L$ ,  $RegA$ , the upper and lower limits of BESS and FESS, and the sign of the ACE signal. This signal controls the input switch to the cumulative discrete block in Fig. 5, so that when  $Clp = 1$ , the switch is set to its upper position, forcing the first filter input to 0 to avoid saturation; otherwise, when  $Clp = 0$ , the switch is set to its lower position, so that the corresponding filter input is the cumulative value of the ACE signal.

In addition,  $BP_{FESS}$  and  $BP_{BESS}$  should be set in the control center; currently these values are close to 0 for the IESO, but can be different if the ESS facilities are also considered for energy arbitrage. The last four inputs of the anti-windup block contain SoC information for the ESS facilities, and since they

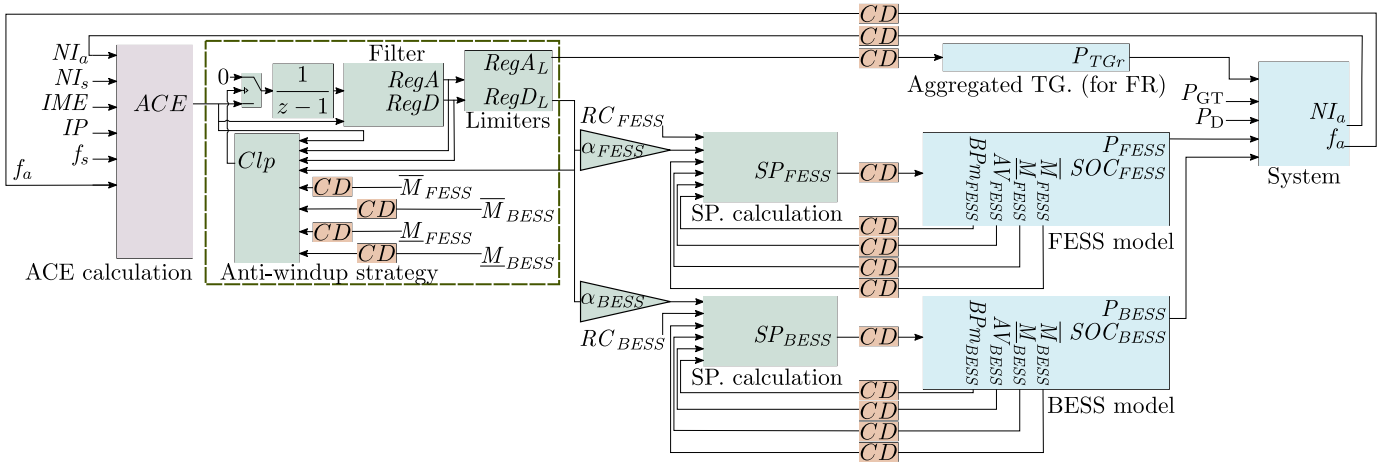


Fig. 5: Filter integration into the Base Case Model of Fig. 1 (Integrated Model).

come from these facilities, a CD is considered.

The proposed filter sends  $RegA$  and  $RegD$  signals considering the SoC of fast resources and capacity limits of ESSs and TGs, and depend on the conditions of the system, working in a coordinated manner. The hard energy neutrality condition or the soft neutrality condition on the  $RegD$  signal, like those implemented in PJM [31], are not included here, to avoid issues such as over procuring fast response resources or having the ESS facilities work against the system FR needs to achieve the hard neutrality condition. The controller proposed here acts to bring the ACE back to zero through an optimal coordinated control between fast and slow resources, thus optimizing the use of those resources while considering system limitations. Furthermore, since the ESS are exclusively being used for FR, there is no need to force this signal to meet an energy neutral condition, from the ISO perspective.

The SP calculation in [26] is modified here so that the FR capacity from FESS and BESS can be significant as compared to the TGs FR capacity, which is not the case in [26], where these are assumed to be small. The ESS facilities are considered to have different capacity limits here; thus, the FR signal  $RegDL$  sent to FESS and BESS is multiplied by a factor  $\alpha_{FESS}$  or  $\alpha_{BESS}$  for FESS or BESS, respectively ( $\alpha_{FESS} + \alpha_{BESS} = 1$ ), which indicate their respective capacity contributions to the total ESS capacity required for FR. Accordingly, the SP calculation in Fig. 1 is modified in the PSP blocks as follows:

$$SP_{ESS} = \begin{cases} 0 & \forall AV_{ESS} = 1, \alpha_{ESS}RegDL \geq 0, \\ & \quad \bar{M}_{ESS} = BP_{ESS} \\ 0 & \forall AV_{ESS} = 1, \alpha_{ESS}RegDL < 0, \\ & \quad \underline{M}_{ESS} = BP_{ESS} \\ \alpha_{ESS}RegDL & \forall AV_{ESS} = 1, RC_{ESS} \neq 0, \\ & \quad \underline{M}_{ESS} \neq BP_{ESS}, \bar{M}_{ESS} \neq BP_{ESS} \\ \alpha_{ESS}RegDL & \forall AV_{ESS} = 1, RC_{ESS} \neq 0, \\ & \quad \alpha_{ESS}RegDL \geq 0, \bar{M}_{ESS} \neq BP_{ESS} \\ \alpha_{ESS}RegDL & \forall AV_{ESS} = 1, RC_{ESS} \neq 0, \\ & \quad \alpha_{ESS}RegDL < 0, \underline{M}_{ESS} \neq BP_{ESS} \end{cases} \quad (5)$$

In this calculation, the ESS SP signal  $SP_{ESS}$  for either FESS

or BESS is equal to 0 or  $\alpha_{ESS}RegDL$  depending on the values of  $AV_{ESS}$ ,  $\alpha_{ESS}RegDL$ ,  $RC_{ESS}$ , and the facility's SoC, included in the signals  $\bar{M}_{ESS}$  and  $\underline{M}_{ESS}$ . If the  $\alpha_{ESS}RegDL$  signal indicates that the facility should charge or discharge, but this is not possible from the SoC management perspective, the SP is set to 0. Otherwise,  $SP_{ESS}$  is equal to  $\alpha_{ESS}RegDL$ . An idle state of the ESS, which has not been considered before, is enforced through this PSP calculation.

The proposed filter produces two different signals,  $RegA$  and  $RegD$ , with similar characteristics to the current PJM FR approach. However, the proposed strategy has the following main advantages over the current PJM signals. First, the proposed  $RegA$  and  $RegD$  are the result of an optimal control design problem which incorporates the aggregated dynamics of traditional FR resources, along with approximate CDs and an aggregated model of the bulk power system. Incorporation of the dynamic effects directly in the design stage leads to improved closed-loop response. Second, the PJM neutrality condition, which caused over procuring issues in PJM, is not included here.

Since the proposed approach takes advantage of the ESS high ramp rates, the  $\mathcal{H}_2$  anti-windup method, and PSP calculation could be implemented in ISOs that have adopted FERC Order 755, such as MISO, CAISO, ISONE, NYISO, and others, to take advantage of the fast regulation resources that are currently part of their regulation markets and to coordinate traditional and fast resources. These ISOs have already modified their market structure to include ESS fast power responses, calculating the mileage and including a performance factor, which can be obtained from the  $RegD$  signal of the proposed filter. In addition, the proposed integrated model can be used to determine different regulation capacities for both conventional and fast response resources and a conversion factor between regulation products, as in PJM [4].

#### IV. SIMULATION STUDIES

This section presents the simulation results of the proposed Integrated and Base Case Models for the OPS, for comparison purposes. For the cases considering limited FR capacity, the assumed scheduled capacity is  $\pm 100$  MW and  $\pm 50$  MW from

TGs and ESS, respectively, since currently, the IESO schedules a minimum of  $\pm 100$  MW from TGs and  $\pm 7.05$  MW from ESS. This assumed ESS regulation capacity includes a 25 MW/6.25 MWh FESS and a 25 MW/50 MWh BESS (currently these are 2 MW/0.5 MWh for FESS, and 4 MW/2.76 MWh for BESS). The values of  $\alpha_{FESS}$  and  $\alpha_{BESS}$  are both 0.5, because both FESS and BESS are assumed to have the same capacity. The FESS and BESS models can be dispatched for energy with  $BP_{ESS} > 0$  [26]; in the present studies,  $BP_{ESS} = 0$  and thus the total available capacity is used for regulation, as this is the current practice at the IESO. For visualization purposes, a window of 8000 seconds is considered for all the simulation studies.

The values chosen for the  $\Phi_{W_i}(z)$  filters for the OPS studies are the following, based on the highest change on the corresponding input:

$$\begin{aligned} \Phi_{W_1}(z) &= 1000 \text{ MW}, \quad \Phi_{W_2}(z) = 1000 \text{ MW}, \\ \Phi_{W_3}(z) &= -\frac{1000 \text{ MW}}{B}, \quad \Phi_{W_4}(z) = 1000 \text{ MW}, \\ \Phi_{W_5}(z) &= 100 \text{ MW}, \quad \Phi_{W_6}(z) = 100 \text{ MW} \end{aligned} \quad (6)$$

where  $B$ , i.e., the BA bias, is 2,482 MW/Hz [26].

The optimal values of the GA process for the  $\Phi_{Z_j}(z)$  obtained for the OPS are as follows:

$$\begin{aligned} \Phi_{Z_1}(z) &= 384.97, \quad \Phi_{Z_2}(z) = 9567.88 \frac{0.99z - 0.99}{z - 0.99}, \\ \Phi_{Z_3}(z) &= 77967.58 \frac{0.0016z + 0.0016}{z - 0.99}, \quad \Phi_{Z_4}(z) = 751.5 \end{aligned} \quad (7)$$

The matrices  $A$ ,  $B$ ,  $C$ , and  $D$  defined in Section III-A can be found in [32]. These matrices are used to obtain the controllers  $\Phi(z)$  for all the cases presented in this section.

It is important to mention that the real data used for the simulations in this section correspond to the following signals of April 1st, 2019:  $f_s$ ,  $NI_s$ ,  $IME$ ,  $IP$ ,  $P_{GT}$ , and  $P_D$ . This data has been provided by the IESO and has been re-sampled to 1 s resolution.

#### A. Impact of CDs

When CDs are ignored, the FR signals are calculated at the control center at time  $t$ , and sent to the FR facilities, which are immediately received by them, and their responses sent back instantly to the control center. The TGs and ESS facilities act on these FR signals, reducing the ACE. However, CDs exist in the FR process and thus the ACE is not corrected instantly; hence, the error keeps accumulating and more regulation resources are needed to correct it. Ignoring CDs in real systems can potentially lead to errors in determining the FR capacity needed and the impact of regulating resources in reducing the ACE.

Fig. 6 and Fig. 7 presents the Base Case and Integrated Model results considering limited FR capacity without and with CDs of  $\tau = 4s$  for most signals, and  $\tau = 30s$  for the TG regulation signal, as it is currently the case in Ontario. Note the significant reduction in ACE in Fig. 6 due to the absence of CDs. The proposed filter, included in the Integrated Model, takes into account CDs in the design process and in the system to send appropriate FR signals. Observe that  $P_{FESS}$

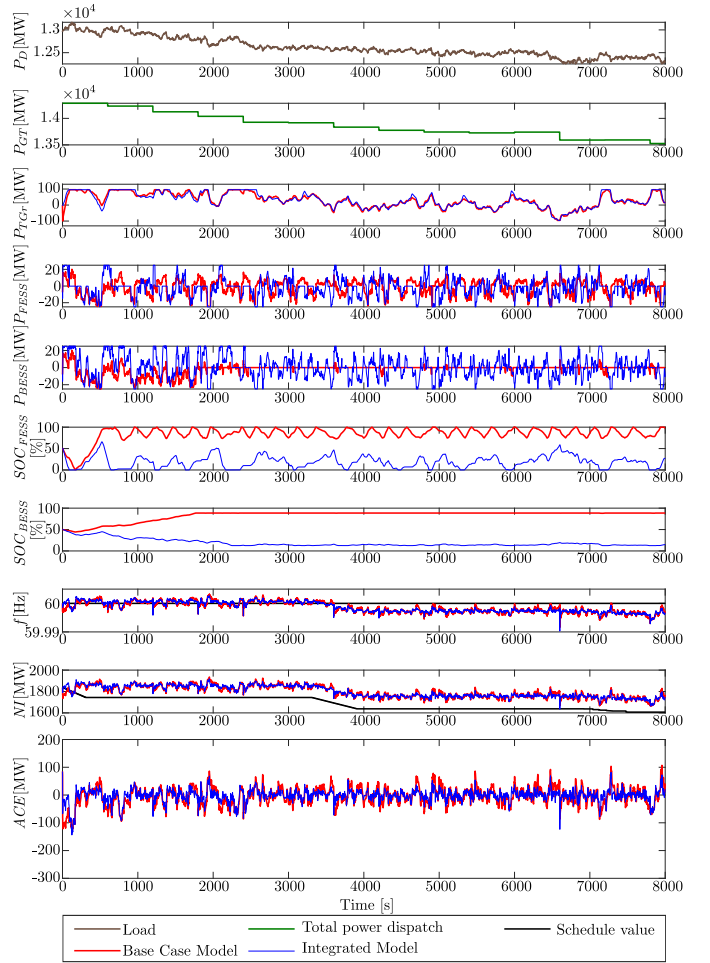


Fig. 6: Base Case Model and Integrated Model comparison for limited FR capacity and without considering CDs.

TABLE I: Impact of CDs on the FR process.

Case	RMSE [MW]	MAE [MW]	Mean [MW]	SD [MW]
No CDs				
Base Case Model limited FR cap.	32.57	25.16	-4.60	32.24
Integrated Model limited FR cap.	21.79	14.52	-2.22	21.68
With CDs				
Base Case Model limited FR cap.	46.35	36.45	-6.15	45.94
Integrated Model limited FR cap.	38.45	29.73	-3.18	38.32

and  $P_{BESS}$ , which are the response of FESS and BESS to  $RegD$ , move faster in the Integrated Model than the Base Case, while the  $P_{TGr}$  signal in both models is similar.

Table I presents the RMSE and MAE of the ACE signal measured with respect to the ideal ACE (i.e., 0 MW), and the mean and Standard Deviation (SD) of the same signal for the Base Case and Integrated Models without and with CDs. The MAE of the Integrated Model is 58% and 82% of the error of the Base Case Model without and with CDs, respectively. In addition, the RMSE, mean, and SD are closer to zero for the cases with the Integrated Model, specially for the case without CDs. These results highlight the importance of CDs in the FR process. Certainly, by eliminating or at least reducing

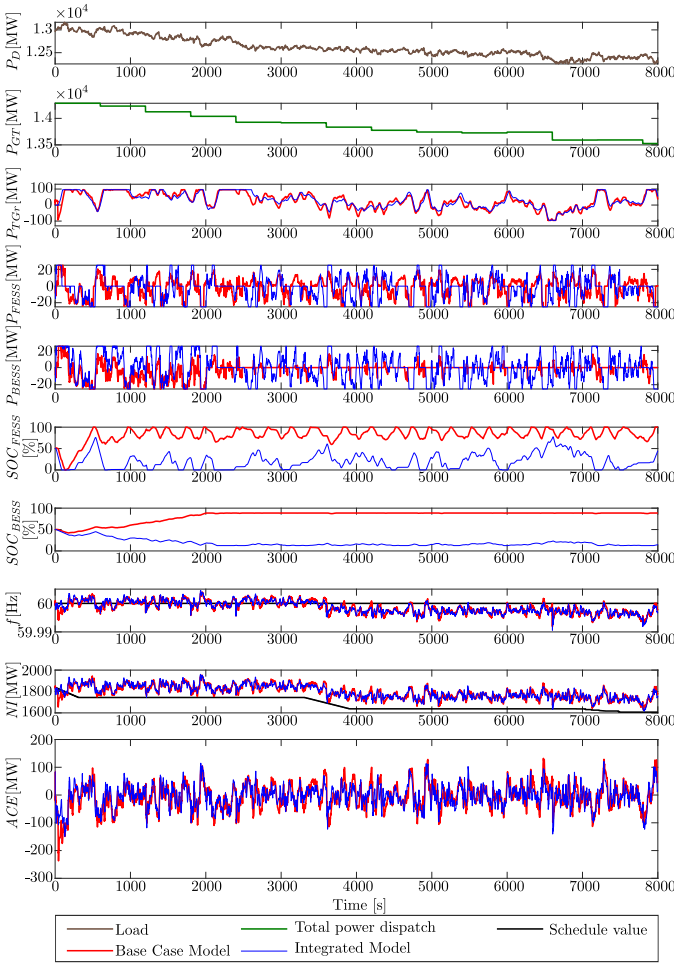


Fig. 7: Base Case Model and Integrated Model comparison for limited FR capacity and considering CDs.

TABLE II: Impact of regulation capacity limit on the FR process.

Case	RMSE [MW]	MAE [MW]	Mean [MW]	SD [MW]
No CDs				
Base Case Model untd. FR cap.	231.45	229.36	-1.28	231.46
Integrated Model untd. FR cap.	13.53	10.39	-0.01	13.53
Base Case Model ltd. FR cap.	32.57	25.16	-4.60	32.24
Integrated Model ltd. FR cap.	21.79	14.52	-2.22	21.68
With CDs				
Base Case Model untd. FR cap.	1632	1505	-1.40	1632
Integrated Model untd. FR cap.	31.33	24.35	-0.06	31.32
Base Case Model ltd. FR cap.	46.35	36.45	-6.15	45.94
Integrated Model ltd. FR cap.	38.45	29.73	-3.18	38.32

CDs, the ACE can be improved by up to 42% without adding extra FR capacity. It should be mentioned that for the case of the system without CDs, the delays were ignored in the filter design process, while for the case with CDs, these were considered.

### B. Impact of Limited Regulation Capacity

Fig. 6 and Fig. 8 present the results of the Base Case and Integrated Models considering limited and unlimited FR

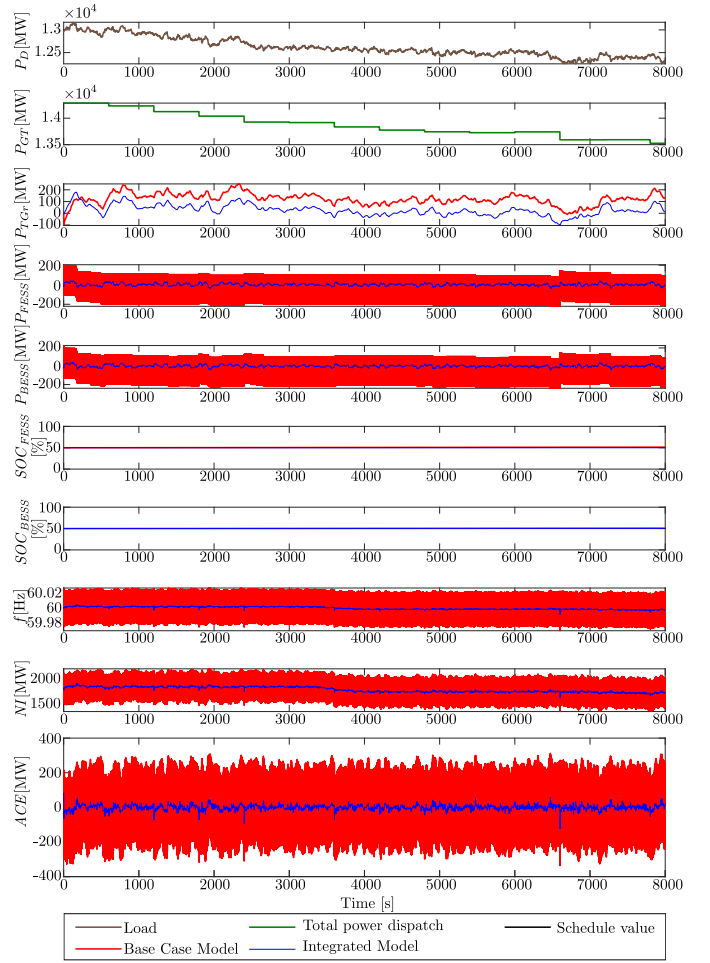


Fig. 8: Base Case Model and Integrated Model comparison for unlimited FR capacity and without considering CDs.

capacity, respectively, and no CDs; likewise, Fig. 7 and Fig. 9 present the two cases considering CDs in the FR process. For unlimited FR capacity without and with CDs, note in Fig. 8 and Fig. 9 that the Base Case becomes unstable. This happens because  $RegA$  and  $RegD$  are generated independent of each other, resulting in an uncoordinated operation of the FR resources. A similar FR signal is sent to the AGC block, where the  $RegA$  is calculated, and sent to the SP calculation blocks, where  $SP_{FESS}$  and  $SP_{BESS}$  are calculated, which are basically the same signal scaled to each facility's capacity, but since unlimited capacity is considered, the entire  $RegD$  is sent to both FESS and BESS. Hence, at every time interval, three times the FR requirement is requested from the regulation facilitates (TGs, FESS, and BESS); such overcompensation creates a regulation requirement in the opposite direction of the error on top of the generation-load mismatches for the next time interval. This keeps happening at every time interval making the system unstable. The situation is worse when CDs are considered, since the ACE keeps accumulating due to overcompensation of regulation resources and also due to the delays in the response from facilities contracted for FR.

Table II presents the RMSE, MAE, mean, and SD of the ACE signal related to all cases with limited and unlimited FR capacity and without and with CDs. The Integrated Model

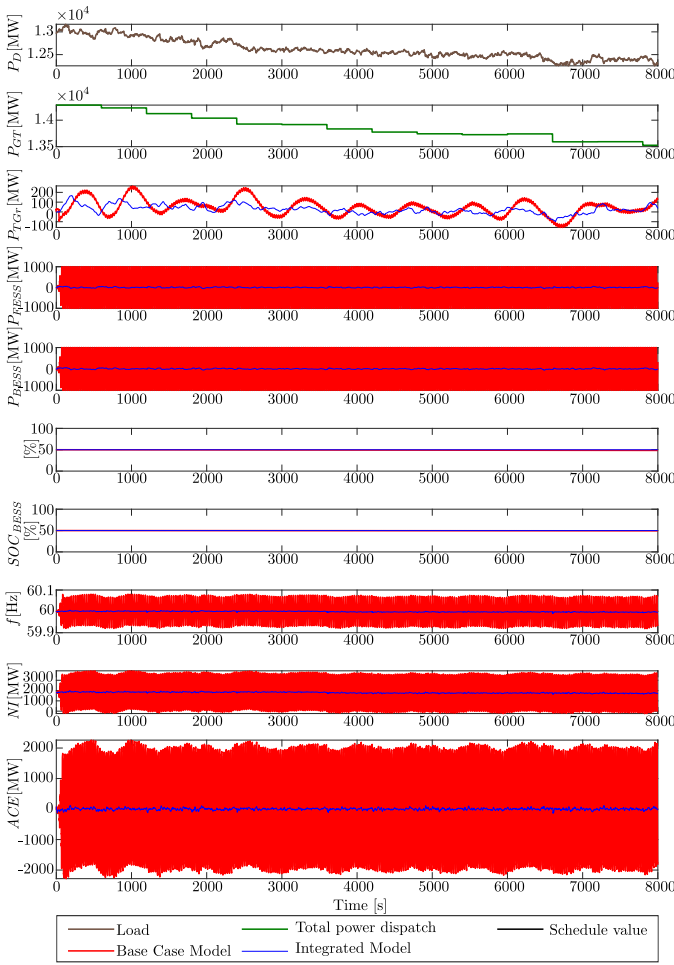


Fig. 9: Base Case Model and Integrated Model comparison for unlimited FR capacity and considering CDs.

yields better results compared to the Base Case Model under the same conditions, in all the cases. In addition, as expected, when unlimited FR resource capacity is considered in the Integrated Model, the RMSE, MAE, mean, and SD of the ACE are close to zero compared to the cases with limited FR resources. The ideal case presented in this table corresponds to the Integrated Model considering unlimited FR capacity and no CDs. However, the ACE is not zero in this case because the TGs have a time response characteristic that causes some accumulation of the ACE. The MAE is reduced by 72% compared to the Base Case Model using limited FR capacity and considering CDs. Even though the ideal case may not be achievable due to impossibility to eliminate all CDs, this result provides an idea of the maximum improvement in the FR process, measured as a reduction in the ACE profile.

Considering unlimited capacity in the Integrated Model and analyzing the maximum regulation requirement allows for overall power sizing of traditional and fast regulation requirements to achieve optimal ACE reduction. Thus, when analyzing the case with CDs, the maximum regulation capacities from TGs, FESS, and BESS are  $\pm 167$  MW,  $\pm 61$  MW, and  $\pm 61$  MW, respectively, while for the case without CDs the maximum required capacities are  $\pm 180$  MW,  $\pm 42$  MW, and  $\pm 42$  MW, respectively. These capacities are for a time

TABLE III: Impact of TG capacity on FR for the proposed  $\mathcal{H}_2$  filter.

Case	RMSE [MW]	MAE [MW]	Mean [MW]	SD [MW]
Base Case Model with limited FR capacity and CDs				
100 MW TGs, 50 MW ESSs	46.35	36.45	-6.15	45.94
Integrated Model with limited FR capacity and CDs				
100 MW TGs, 50 MW ESSs	38.45	29.73	-3.18	38.32
90 MW TGs, 50 MW ESSs	38.73	29.96	-3.86	38.53
80 MW TGs, 50 MW ESSs	39.65	30.42	-4.71	39.37
70 MW TGs, 50 MW ESSs	40.52	30.71	-5.61	40.13
60 MW TGs, 50 MW ESSs	41.50	31.28	-7.30	40.86
50 MW TGs, 50 MW ESSs	42.47	31.68	-9.16	41.48

interval of 8000 s, but longer time periods could be analyzed following the same procedure.

The proposed filter has the potential to impact the FR capacity required by the system, as a comparison of the results shows for the Base Case Model and Integrated Model with limited capacity and CDs, which reflect the existing system FR limitations. Thus, varying FR capacities for TGs were considered, while keeping the ESSs' capacities fixed at 50 MW, as shown in Table III. Note that when the total FR capacity is reduced by 30 MW of the Integrated Model, i.e., for 70 MW of TG capacity, the RMSE, MAE, Mean, and SD for the ACE are closer to zero compared to the Base Case Model. Observe also that, even by reducing 50 MW of FR TG capacity in the Integrated Model, most of the results in Table III are closer to zero than the ones obtained for the Base Case Model.

The IESO spent \$51,197,491 in FR for the period of January 1, 2019, to December 31, 2019, scheduling typically  $\pm 100$  MW of TG at all times [28]; thus, the approximate cost of 1 MW of scheduled FR capacity would be \$511,975. Assuming that similar and possible better system FR can be accomplished with the planned  $\pm 150$  MW total FR capacity of slow and fast resources considered in Table III, for the same period and at the same cost per MW, the total FR costs would be \$76,796,250. Therefore, by implementing the proposed filter, which would allow to reduce the FR capacity by at least 30 MW, as it improves the system FR with respect to the Base Case Model, the total potential savings for the IESO would be \$15,359,250. This potential savings only relates to the operational costs of the system without considering further potential savings due to additional infrastructure requirements or economic benefits of lower ACE values. In spite of the broad assumptions made on this calculation, the likely cost savings demonstrate the possible economic benefits, besides the technical ones, of the proposed filter.

### C. Effect of Proposed ESS Set-point Calculation

The effect of the PSP calculation using the Integrated Model is presented in Fig. 10, and considers CDs and limited FR capacity. The RMSE, MAE, mean, and SD of the ACE for the Base Case, which uses SP calculation, and the Integrated Model with the SP and PSP calculation, are presented in Table IV. Although, the SP calculation in the Integrated Model

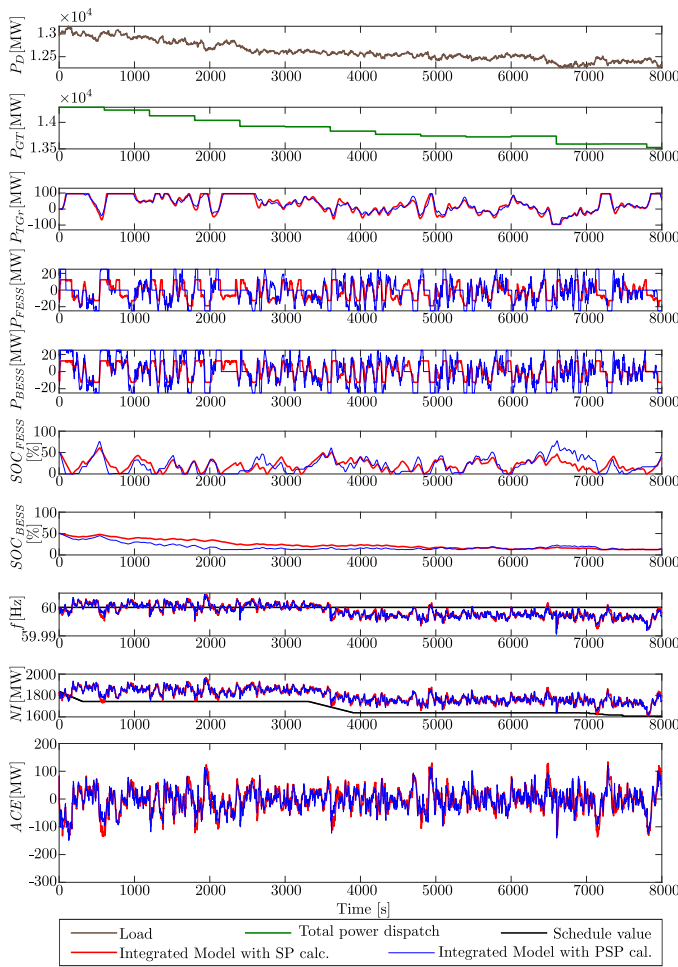


Fig. 10: Integrated Model with SP and PSP calculation comparison for limited FR capacity and considering CDs.

TABLE IV: Impact of PSP calculation in the FR process.

Case	RMSE [MW]	MAE [MW]	Mean [MW]	SD [MW]
Base Case Model SP calculation	46.35	36.45	-6.15	45.94
Integrated Model SP calculation	44.00	34.06	-3.71	43.85
Integrated Model PSP calculation	38.45	29.73	-3.18	38.32

TABLE V: Impact of anti-windup strategy on the FR process.

Case	RMSE [MW]	MAE [MW]	Mean [MW]	SD [MW]
Base Case Model	46.35	36.45	-6.15	45.94
Integrated M. without anti-windup	40.88	31.45	-0.28	40.88
Integrated M. with anti-windup	38.45	29.73	-3.18	38.32

provides smaller errors as compared to the Base Case, the PSP calculation in the Integrated Model yields better results and allows taking advantage of the coordinated control provided by the proposed  $\mathcal{H}_2$  filter strategy.

#### D. Effect of Proposed Anti-windup Strategy

Fig. 11 presents a comparison of the Integrated Model without and with the proposed anti-windup strategy explained in Section III-B. Although, the Integrated Model ignoring or

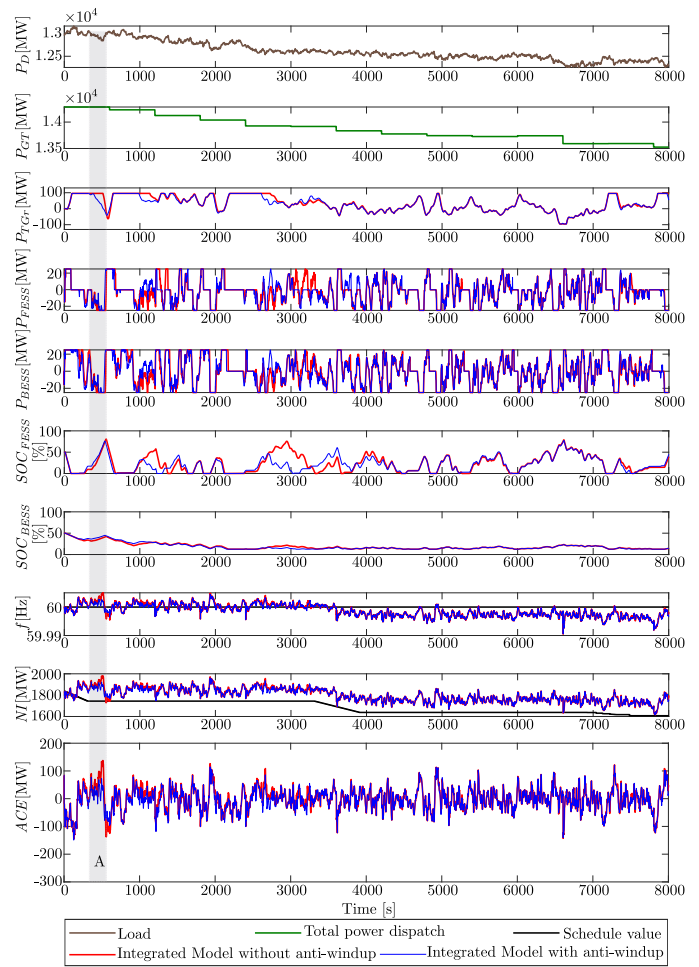


Fig. 11: Integrated Model with and without anti-windup strategy comparison for limited FR capacity and considering CDs.

including the anti-windup strategy yields better ACE than the Base Case, as shown in Table V, the anti-windup strategy reduces the ACE further by avoiding saturation when all the facilities reach their limits, or when the TGs are at their capacity limits and the ESS cannot follow  $RegD$  due to their SoC. An example of the effect of the anti-windup strategy when saturation occurs is highlighted in the shaded area A in Fig. 11, where the saturation condition and the lack of anti-windup strategy yields a larger ACE as compared to the case with anti-windup. Since saturation cases can occur several times during the day, the presence of the anti-windup strategy is essential to take full advantage of the proposed  $\mathcal{H}_2$  filter.

The standard filter design method used in this paper guarantees local stability and robustness of the overall system [29]. Thus, the Integrated Model was designed to be locally stable, which is confirmed by the results of the simulations depicted in Fig. 6 to Fig. 11. In particular, Fig. 8 and Fig. 9 show that the overall nonlinear system that includes the designed filter is stable and robust, since it stabilizes the system under the conditions that cause instability in the Base Case Model.

## V. CONCLUSIONS

This paper presented an optimized  $\mathcal{H}_2$  filter strategy to split the FR signal into a slow  $RegA$  signal sent to TGs, and a

fast  $RegD$  signal sent to ESSs, to take advantage of the fast response characteristics of FESS and BESS. The proposed  $\mathcal{H}_2$  filter strategy was implemented in a previously validated FR model of the OPS. The quantification of the impact of the proposed filter strategy on the FR performance was measured in terms of the reduction in ACE. Simulation results for the OPS showed that, in all cases, the proposed filter yielded better results as compared to the existing FR process. It was noted that CDs negatively affected the FR process and a 60% reduction in the MAE of ACE was achieved by adding the proposed filter strategy, eliminating the CDs, with the same FR capacity; the proposed filter produced FR signals that worked in a coordinated manner avoiding instability in the system. Furthermore, it was shown that the proposed Integrated Model could be used for sizing of FR facilities by assuming unlimited ESS capacity. A PSP calculation method and anti-windup strategy were also proposed to take full advantage of the novel  $\mathcal{H}_2$  filter strategy, demonstrating their relevance for the FR process. From the ISO perspective, the participation of ESS and the proposed filtering strategy can improve the performance of the regulation process and reduce the overall capacity requirement for FR services.

## REFERENCES

- [1] C. Mu, Y. Zhang, H. Jia, and H. He, "Energy-storage-based intelligent frequency control of microgrid with stochastic model uncertainties," *IEEE Trans. Smart Grid*, vol. 11, no. 2, pp. 1748–1758, Mar. 2020.
- [2] "Frequency regulation compensation in the organized wholesale power markets," FERC, Order No. 755, Dockets RM11-7-000 AD10-11-000.
- [3] L. Meng, J. Zafar, S. K. Khadem, A. Collinson, K. C. Murchie, F. Coffele, and G. M. Burt, "Fast frequency response from energy storage systems—A review of grid standards, projects and technical issues," *IEEE Trans. Smart Grid*, vol. 11, no. 2, pp. 1566–1581, Mar. 2020.
- [4] "Kermite study report to determine the effectiveness of the AGC in controlling fast and conventional resources in the PJM frequency regulation market," KEMA Inc., Chalfont, PA, USA, Tech. Rep., Dec. 2011.
- [5] Toronto, ON, CA, Tech. Rep., Mar. 2016.
- [6] "Electric storage participation in markets operated by regional transmission organizations and independent system operators," FERC, May 2019, Order No. 841-A, Docket Nos. RM16-23-001, AD16-20-001.
- [7] M. Kintner-Meyer, "Regulatory policy and markets for energy storage in North America," *Proc. IEEE*, vol. 102, no. 7, pp. 1065–1072, Jul. 2014.
- [8] A. E. Brooks and B. C. Lesieutre, "A review of frequency regulation markets in three U.S. ISO/RTOs," *The Electricity Journal*, vol. 32, no. 10, p. 106668, Nov. 2019.
- [9] Y. Chen, R. Leonard, M. Keyser, and J. Gardner, "Development of performance-based two-part regulating reserve compensation on MISO energy and ancillary service market," *IEEE Trans. Power Syst.*, vol. 30, no. 1, pp. 142–155, Jan. 2015.
- [10] "Removing obstacles for storage resources in Ontario," IESO, Toronto, ON, CA, Tech. Rep., Dec. 2018.
- [11] B. Xu, Y. Dvorkin, D. S. Kirschen, C. A. Silva-Monroy, and J. Watson, "A comparison of policies on the participation of storage in U.S. frequency regulation markets," in *IEEE Power and Energy Society General Meeting*, Boston, MA, USA, 2016, pp. 1–5.
- [12] Z. Zhou, T. Levin, and G. Conzelmann, "Survey of U.S. ancillary services markets," Argonne National Lab., Argonne, IL, USA, Tech. Rep., Jan. 2016.
- [13] "Implementation and rationale for PJM's conditional neutrality regulation signals," PJM, Toronto, ON, CA, Tech. Rep., Jan. 2017.
- [14] O. Leitermann, "Energy storage for frequency regulation on the electric grid," Ph.D. dissertation, MIT, Cambridge, MA, Jun. 2012.
- [15] J. W. Shim, G. Verbič, N. Zhang, and K. Hur, "Harmonious integration of faster-acting energy storage systems into frequency control reserves in power grid with high renewable generation," *IEEE Trans. Power Syst.*, vol. 33, no. 6, pp. 6193–6205, Nov. 2018.
- [16] K. Doenges, I. Egido, L. Sigrist, E. Lobato Miguélez, and L. Rouco, "Improving AGC performance in power systems with regulation response accuracy margins using battery energy storage system (BESS)," *IEEE Trans. Power Syst.*, vol. 35, no. 4, pp. 2816–2825, Jul. 2020.
- [17] Y. Cheng, M. Tabrizi, M. Sahni, A. Povedano, and D. Nichols, "Dynamic available AGC based approach for enhancing utility scale energy storage performance," *IEEE Trans. Smart Grid*, vol. 5, no. 2, pp. 1070–1078, Mar. 2014.
- [18] S. Pulendran and J. E. Tate, "Capacity scheduling of energy storage and conventional generation for frequency regulation based on CPS1," *IEEE Trans. Power Syst.*, vol. 35, no. 1, pp. 405–414, Jan. 2020.
- [19] S. K. Sahoo and N. K. Kishore, "Battery state-of-charge-based control and frequency regulation in the MMG system using fuzzy logic," *IET Gener. Transm. Distrib.*, vol. 14, no. 14, pp. 2698–2709, Jul. 2020.
- [20] S. Prasad, S. Purwar, and N. Kishor, "H-infinity based non-linear sliding mode controller for frequency regulation in interconnected power systems with constant and time-varying delays," *IET Gener. Transm. Distrib.*, vol. 10, no. 11, pp. 2771–2784, Aug. 2016.
- [21] A. Gomez-Exposito, A. Conejo, and C. Canizares, *Electric energy systems analysis and operation*. Boca Raton, FL, USA: CRC Press, 2018.
- [22] NERC Resources Subcommittee, "Balancing and frequency control," NERC, Princeton, NJ, USA, Tech. Rep., Jan. 2011.
- [23] H. Zhao, M. Hong, W. Lin, and K. A. Loparo, "Voltage and frequency regulation of microgrid with battery energy storage systems," *IEEE Trans. Smart Grid*, vol. 10, no. 1, pp. 414–424, Jan. 2019.
- [24] F. Nadeem, S. M. S. Hussain, P. K. Tiwari, A. K. Goswami, and T. S. Ustun, "Comparative review of energy storage systems, their roles, and impacts on future power systems," *IEEE Access*, vol. 7, pp. 4555–4585, Jan. 2019.
- [25] A. Akhil, G. Huff, A. Currier, B. Kaun, D. Rastler, S. Chen, A. Cotter, D. Bradshaw, and W. Gauntlett, "DOE/EPRI electricity storage handbook in collaboration with NRECA," Sandia National Laboratories, Albuquerque, NM, USA, Tech. Rep., Jul. 2013.
- [26] N. S. Guzman, C. A. Cañizares, K. Bhattacharya, and D. Sohm, "Frequency regulation model of bulk power systems with energy storage," *ArXiv e-prints*, Sep. 2020, arXiv:2009.04573 [eess.SY].
- [27] 2020 Year in Review. IESO.ca. (Accessed: February 16<sup>th</sup>, 2021). [Online]. Available: <https://www.ieso.ca/en/corporate-ieso/media/year-end-data>
- [28] Ancillary Services Market. IESO.ca. (Accessed: January 29<sup>th</sup>, 2021). [Online]. Available: <https://www.ieso.ca/ancillary-services>
- [29] Skogestad, S. and Postlethwaite, I., *Multivariable Feedback Control Analysis and Design*, 2nd ed. John Wiley and Sons, 2005.
- [30] Matlab. Mathworks.com. (Accessed: August 26<sup>th</sup>, 2020). [Online]. Available: <https://www.mathworks.com/products/matlab.html>
- [31] T. Lee, "Energy storage in PJM: Exploring frequency regulation market transformation," Kleinman Center for Energy Policy, Philadelphia, PA, USA, Tech. Rep., Jul. 2017.
- [32] N. S. Guzman, M. Arriaga, C. Cañizares, J. W. Simpson-Porco, D. Sohm, and K. Bhattacharya, "Regulation signal design and fast frequency control with energy storage systems: Generalized plant state-space matrices (with and without delays)," 2021. [Online]. Available: <https://dx.doi.org/10.21227/g7m4-0z19>



**Noela Sofia Guzman E.** (S'13) received the B.Sc. degree (Summa Cum Laude) in electrical engineering from Escuela Politecnica Nacional (EPN), Quito, Ecuador, in 2014. From 2014 to 2016 she worked as technical assistant at the Electricity Corporation of Ecuador - Business Unit Transelectric, Quito, Ecuador. She is currently pursuing the Ph.D. degree at the Department of Electrical and Computer Engineering, University of Waterloo, Ontario, Canada. Her current research interests include power systems, modeling, optimization, frequency regulation,

and energy storage systems.



**Mariano Arriaga** (S'11-M'15) received the B.A.Sc. and M.A.Sc. degrees in industrial systems engineering from the University of Regina, Canada, in 2003 and 2004, respectively. He received the M.Sc. degree in renewable energy from the University of Zaragoza, Spain, in 2009., and the Ph.D. degree in Electrical and Computer Engineering from the University of Waterloo in 2015. He is the General Manager at the Energy & Power Innovation Centre at Mohawk College, Hamilton, Ontario. Previously, Dr. Arriaga worked as a postdoctoral fellow at the

University of Waterloo, as well as industry and research positions in the oil/gas, automotive and renewable energy industries. At the Centre, Dr. Arriaga's applied research activities include renewable energy integration, microgrids, protection & control, and industrial communications. Dr. Arriaga is a Registered Professional Engineer in the province of Ontario.



**Kankar Bhattacharya** (M'95-SM'01-F'17) received the Ph.D. degree in electrical engineering from the Indian Institute of Technology Delhi, New Delhi, India, in 1993. He was with the Faculty of Indira Gandhi Institute of Development Research, Mumbai, India, from 1993 to 1998, and with the Department of Electric Power Engineering, Chalmers University of Technology, Gothenburg, Sweden, from 1998 to 2002. In 2003, he joined the Electrical and Computer Engineering Department, University of Waterloo, Waterloo, ON, Canada, where he is

currently a Full Professor. His current research interests include power system economics and operational aspects. He is a Registered Professional Engineer in the province of Ontario.



**Claudio Cañizares** (S'85-M'91-SM'00-F'07) is a University Professor and Hydro One Endowed Chair at the ECE Department of the University of Waterloo, where he has been since 1993. His highly cited research focuses on modeling, simulation, computation, stability, control, and optimization of power and energy systems. He is the IEEE Trans. Smart Grid EIC; PES Delegate-Elect to the IEEE Board; a Fellow of the IEEE, the Royal Society of Canada, and the Canadian Academy of Engineering; and has received the 2017 IEEE PES Outstanding Power

Engineering Educator Award, the 2016 IEEE Canada Electric Power Medal, and multiple awards and recognitions from PES Technical Committees.



**John W. Simpson-Porco** (S'10-M'15) received the B.Sc. degree in engineering physics from Queen's University, Kingston, ON, Canada in 2010, and the Ph.D. degree in mechanical engineering from the University of California at Santa Barbara, Santa Barbara, CA, USA in 2015. He is currently an Assistant Professor of Electrical and Computer Engineering at the University of Toronto, Toronto, ON, Canada. He was previously an Assistant Professor at the University of Waterloo, Waterloo, ON, Canada and a visiting scientist with the Automatic Control

Laboratory at ETH Zürich, Zürich, Switzerland. His research focuses on feedback control theory and applications of control in modernized power grids. Prof. Simpson-Porco is a recipient of the Automatica Paper Prize, the Center for Control, Dynamical Systems and Computation Best Thesis Award, and the IEEE PES Technical Committee Working Group Recognition Award for Outstanding Technical Report. He is currently an Associate Editor for the IEEE Transactions on Smart Grid



**Daniel Sohm** has 10 years of experience at Independent Electricity System Operator validating equipment performance, simulating events on the power system, managing ancillary service contracts, integrating energy storage into the wholesale electricity market, and performing research related to energy storage and ancillary services. He received a B.A.Sc. degree in Electrical and Computer Engineering from the University of Waterloo in 2011 and a Master of Engineering degree in Electrical and Computer Engineering specializing in Energy Systems from

the University of Toronto in 2018. He is a professional engineer in Ontario, Canada.